Electronic Supplementary Material (ESI) for RSC Advances.

Supplementary Information

NHC Macrometallocycles of Mercury(II) and Silver(I): Synthesis, Structural Studies and Recognition of Hg(II) Complex 4 for Silver ion

Qing-Xiang Liu,* Qing Wei, Rui Liu, Xiao-Jun Zhao and Zhi-Xiang Zhao

Table of contents

1. CCDC numbers for complexes **1**-**8**.

2. Summary of crystallographic data for **1**-**8** (Table S1-Table S3).

3. The dihedral angles of complexes **2**-**8** (Table S4).

4. The distances of π-π interactions, distances (Å) and angles of C-H···π contacts and H-Bonding geometry of complexes **1**-**8** (Table S5, Table S6).

5. The crystal packings of complexes **1**-**8** (Fig. S1-Fig. S8).

6. The UV/Vis and fluorescence studies of complex **4** (Fig. S9-Fig. S12).

7. The infrared spectra of complex **4** and **4**·$AgNO_3$ **(**Fig. S13).

8. The ^{1}H NMR and ^{13}C NMR spectra of precursors and complexes **1-8 (**Fig. S14-Fig. S47).

1. CCDC numbers for complexes 1-8.

CCDC1033244-1033251 contains the supplementary crystallographic data for complexes **1-8**. These data can be obtained free of charge via http//www.ccdc.cam.ac.uk/conts/retrieving.html, or from the Cambridge Crystallographic Data Centre, 12 Union Road, Cambridge, CB2 1EZ, UK; fax: (+44) 1223-336-033; or e-mail: deposit@ccdc.cam.ac.uk.

2. Summary of crystallographic data for **1-8** (Table S1-Table S3).

Table S1 Summary of crystallographic data for **1-3**

	1	**2**	**3**·0.5($C_4H_{10}O$)
chemical formula	$C_{32}H_{34}Cl_6N_4O_2Pd_2$	$C_{160}H_{136}Cl_2Hg_4I_6N_{24}O_8$	$C_{34}H_{36}Cl_2Hg_2I_2N_4O_2$ ·0.5($C_4H_{10}O$)
fw	932.13	4157.59	1295.61
Cryst syst	Orthorhombic	Monoclinic	Monoclinic
space group	*Pbca*	*P*2/*c*	*C*2/*c*
a/Å	11.013(4)	11.563(2)	13.177(1)
b/Å	21.581(8)	15.735(3)	17.859(2)
c/Å	28.993(1)	23.079(4)	18.350(2)
α/deg	90	90	90
β/deg	90	116.4(7)	95.4(2)
γ/deg	90	90	90
V/Å^3	6891.0(4)	3760.3(1)	4298.9(9)
Z	8	1	4
D_{calcd}, Mg/m^3	1.797	1.836	2.002
Abs coeff, mm^{-1}	1.546	5.404	8.729
F(000)	3712	2000	2420
Cryst size, mm	0.18 × 0.17 × 0.16	0.28 × 0.24 × 0.23	0.18 × 0.17 × 0.16
θ_{min}, θ_{max}, deg	2.19, 25.01	1.29, 25.01	1.93, 25.01
T /K	173(2)	296(2)	173(2)
no. of data collected	33822	19214	10716
no. of unique data	6044	6650	3787
no. of refined params	417	461	258
goodness-of-fit on F^2 [a]	1.055	1.029	1.053
Final *R* indices[b] [$I > 2\sigma(I)$]			
*R*1	0.0283	0.0277	0.0460
*wR*2	0.0631	0.0679	0.1283
R indices (all data)			
*R*1	0.0332	0.0363	0.0555
*wR*2	0.0659	0.0719	0.1345

[a] GOF = $[\Sigma\omega(F_o^2 - F_c^2)^2/(n-p)]^{1/2}$, where n is the number of reflection and p is the number of parameters refined. [b] $R_1 = \Sigma(||F_o| - |F_c||)/\Sigma|F_o|$; $wR_2 = [\Sigma[w(F_o^2 - F_c^2)^2]/\Sigma w(F_o^2)^2]^{1/2}$.

Table S2 Summary of crystallographic data for **4-6**

	4·2DMSO·CH_3CN	**5**·CH_3OH	**6**·0.75DMSO
chemical formula	$C_{36}H_{40}HgI_2N_4O_2$ ·2DMSO·CH_3CN	$C_{28}H_{36}HgI_2N_4O_2$ ·CH_3OH	$C_{26}H_{34}Hg_2I_4N_4O_3S$ ·0.75DMSO
fw	1212.42	947.04	1450.01
Cryst syst	Monoclinic	Monoclinic	Monoclinic
space group	$P2_1/c$	$C2/c$	$P2_1/c$
a/Å	15.477(4)	15.437(2)	8.909(3)
b/Å	19.092(5)	15.405(2)	26.074(1)
c/Å	16.200(4)	15.041(2)	17.047(7)
α/deg	90	90.00	90
β/deg	93.1(5)	108.0(2)	97.6(1)
γ/deg	90	90.00	90
V/Å^3	4780(2)	3400.2(9)	3924.8(3)
Z	4	4	4
D_{calcd}, Mg/m^3	1.685	1.850	2.487
Abs coeff, mm^{-1}	4.642	6.375	11.103
F(000)	2368	1808	2688
Cryst size, mm	0.18 × 0.17 × 0.15	0.18 × 0.14 × 0.13	0.18 × 0.17 × 0.16
θ_{min}, θ_{max}, deg	1.32, 25.01	1.92, 25.01	1.56, 25.01
T /K	296(2)	296(2)	296(2)
no. of data collected	24279	8584	20059
no. of unique data	8435	2990	6899
no. of refined params	527	187	440
goodness-of-fit on F^2 [a]	1.030	1.074	1.039
Final R indices[b] [I $2\sigma(I)$]			
R1	0.0459	0.0308	0.0316
wR2	0.1183	0.0860	0.0772
R indices (all data)			
R1	0.0691	0.0336	0.0361
wR2	0.1327	0.0878	0.0795

[a] GOF = $[\Sigma\omega(F_o^2 - F_c^2)^2/(n-p)]^{1/2}$, where n is the number of reflection and p is the number of parameters refined. [b] $R_1 = \Sigma(||F_o| - |F_c||)/\Sigma|F_o|$; $wR_2 = [\Sigma[w(F_o^2 - F_c^2)^2]/\Sigma w(F_o^2)^2]^{1/2}$.

Table S3 Summary of crystallographic data for **7** and **8**

	7	**8**
chemical formula	$C_{40}H_{34}AgF_6N_6O_2P$	$C_{36}H_{40}AgF_6N_4O_2P$
fw	883.57	813.56
Cryst syst	Monoclinic	Monoclinic
space group	$P2_1/c$	$C2/c$
a/Å	15.391(3)	16.501(6)
b/Å	17.539(3)	16.221(6)
c/Å	15.492(3)	15.435(6)
α/deg	90	90
β/deg	119.0(3)	119.0(5)
γ/deg	90	90
V/Å^3	3657.5(1)	3611.0(2)
Z	4	4
D_{calcd}, Mg/m^3	1.605	1.496
Abs coeff, mm^{-1}	0.672	0.671
F(000)	1792	1664
Cryst size, mm	0.18 × 0.17 × 0.16	0.18 × 0.17 × 0.16
θ_{min}, θ_{max}, deg	1.51, 25.01	1.89, 25.01
T /K	173(2)	296(2)
no. of data collected	18489	9168
no. of unique data	6436	3191
no. of refined params	505	229
goodness-of-fit on F^2 [a]	1.039	1.048
Final R indices[b] [$I > 2\sigma(I)$]		
$R1$	0.0450	0.0347
$wR2$	0.1103	0.0921
R indices (all data)		
$R1$	0.0569	0.0387
$wR2$	0.1198	0.0957

[a] GOF = $[\Sigma\omega(F_o^2 - F_c^2)^2 /(n-p)]^{1/2}$, where n is the number of reflection and p is the number of parameters refined. [b] $R_1 = \Sigma(||F_o| - |F_c||)/\Sigma|F_o|$; $wR_2 = [\Sigma[w(F_o^2 - F_c^2)^2]/ \Sigma w(F_o^2)^2]^{1/2}$.

3. The dihedral angles of complexes 2-8

Table S4 In the same ligand of **2-8**, the dihedral angles (˚) between two benzimidazole (or imidazole) rings (A), and the dihedral angles (˚) between naphthalene ring and two imidazole (or benzimidazole) rings (B)

Complexes	A	B
2	50.9(3)	73.5(3), 78.8(4)
3	59.0(9)	80.1(8), 80.8(9)
4	53.6(7)	77.7(1), 79.7(5)
5	50.6(4)	85.0(5), 87.4(5)
6	56.0(6)	68.9(6), 85.1(4)
7	52.1(2)	75.2(3), 82.5(3)
8	56.9(1)	77.7(3), 78.6(3)

4. The distances of π-π stacking interactions, distances (Å) and angles of C-H···π contacts and H-Bonding geometry of complexes 1-8

Table S5 Distances (Å) of π-π stacking interactions, and distances (Å) and angles (°) of C-H···π contacts for **1-8**

Complexes	π-π		C-H···π	
	Face-to-face	Center-to-center	H···π	C-H···π
1	3.362(4) (benzimidazole and naphthalene)	3.596(1) (benzimidazole and naphthalene)	_	_
2	3.478(8) (benzimidazole)	3.629(5) (benzimidazole)	2.823(4) 3.095(4)	163.0(3) 138.9(4)
3	3.518(1) (benzimidazole)	3.817(3) (benzimidazole)	_	_
4	3.646(1) (benzimidazole)	3.860(1) (benzimidazole)	3.156(6)	132.4(8)
5	3.683(9) (imidazole)	4.004(4) (imidazole)	3.041(4)	158.0(4)
6	_	_	2.766(1)	144.5(4)
7	3.433(4) (benzimidazole) 3.314(4) (benzimidazole)	3.376(4) (benzimidazole) 4.035(2) (benzimidazole)	2.997(6)	154.2(2)
8	3.597(4) (benzimidazole)	3.712(9) (benzimidazole)	2.958(9)	129.1(3)

Table S6 H-Bonding Geometry for **1**

	D-H···A	D-H (Å)	H···A (Å)	D···A (Å)	D-H···A (˚)
1	C(1)-H(1A)···Cl(6)^{i}	0.978(3)	2.776(9)	3.734(3)	165.9(2)
	C(30)-H(30)···Cl(2)^{ii}	0.949(3)	2.849(9)	3.474(3)	124.3(1)

Symmetry code: i: *x*, 1 + *y*, *z*, ii: -0.5 + *x*, 1 + *y*, 0.5 - *z* for **1**.

5. The crystal packings of complexes 1-8

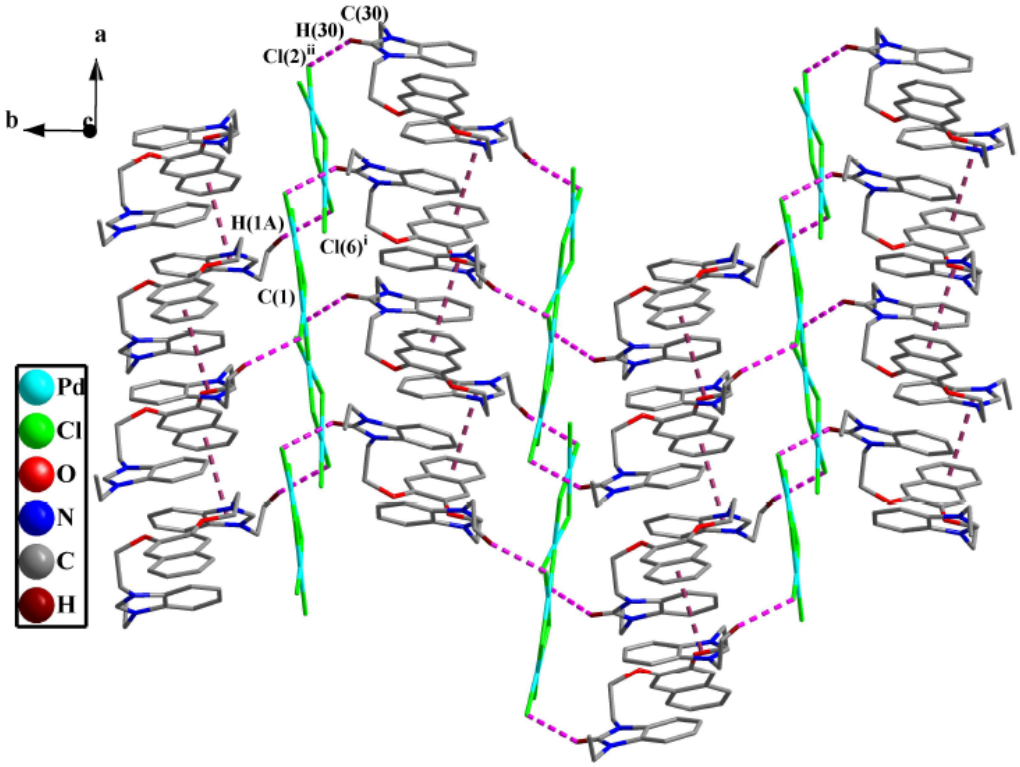

Fig. S1 2D supramolecular layer of complex **1** via π-π stacking interactions and C-H···Cl hydrogen bonds. All hydrogen atoms except those participating in C-H···Cl hydrogen bonds were omitted for clarity.

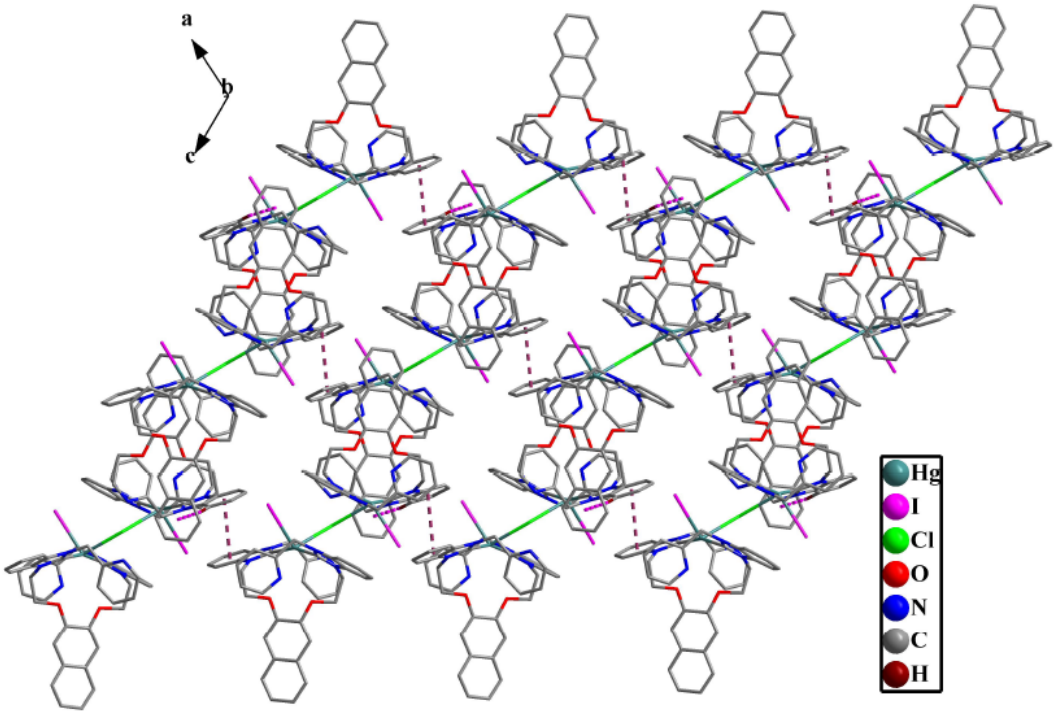

Fig. S2(a) 2D supramolecular layer of complex **2** via C-H···π contacts and π-π stacking interactions. All hydrogen atoms except those participating in C-H···π hydrogen bonds were omitted for clarity.

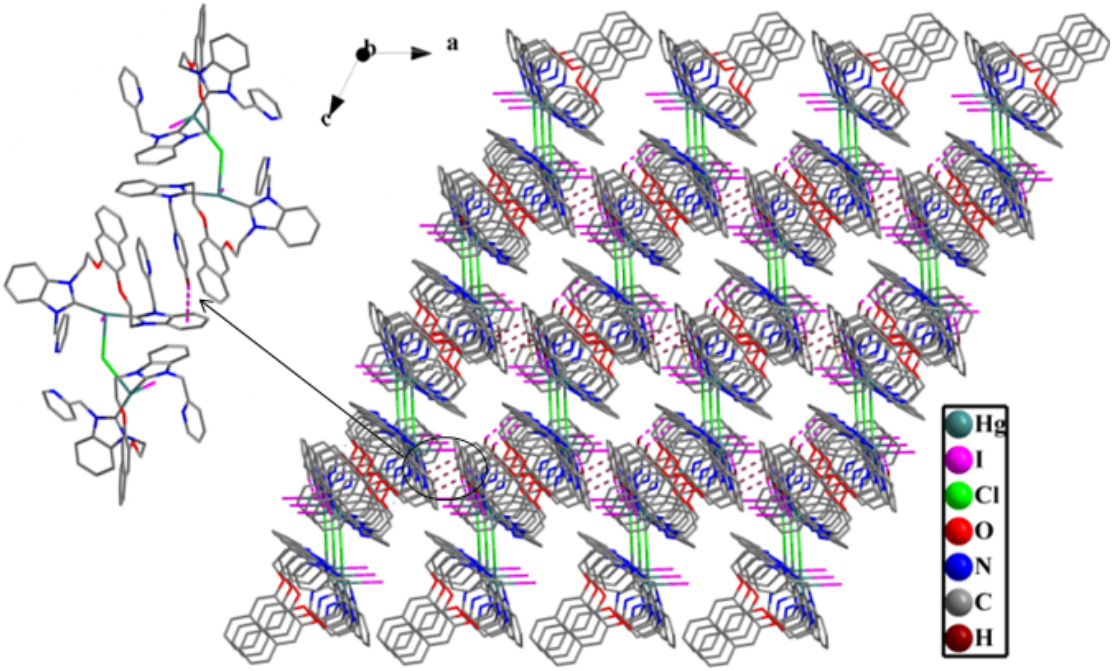

Fig. S2(b) 3D supramolecular network of complex **2** via π-π stacking interactions and C-H···π contacts. All hydrogen atoms except those participating in C-H···π hydrogen bonds were omitted for clarity.

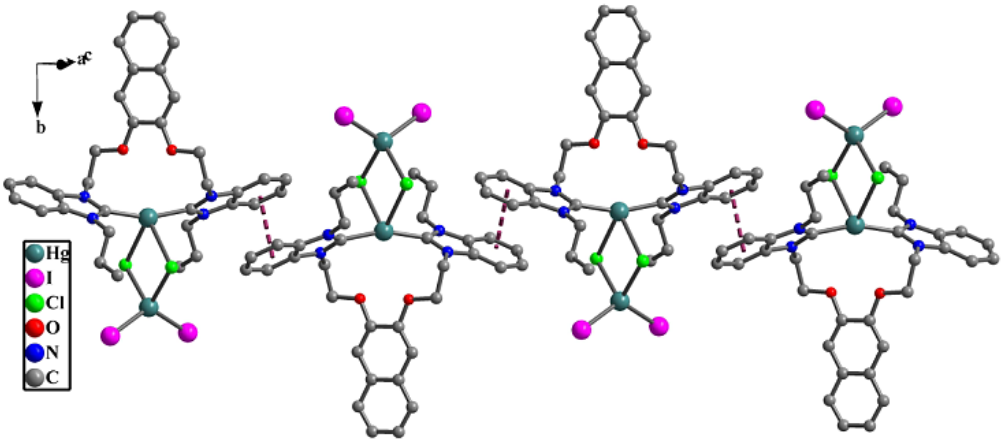

Fig. S3 1D chain of complex **3** via π-π stacking interactions. All hydrogen atoms were omitted for clarity.

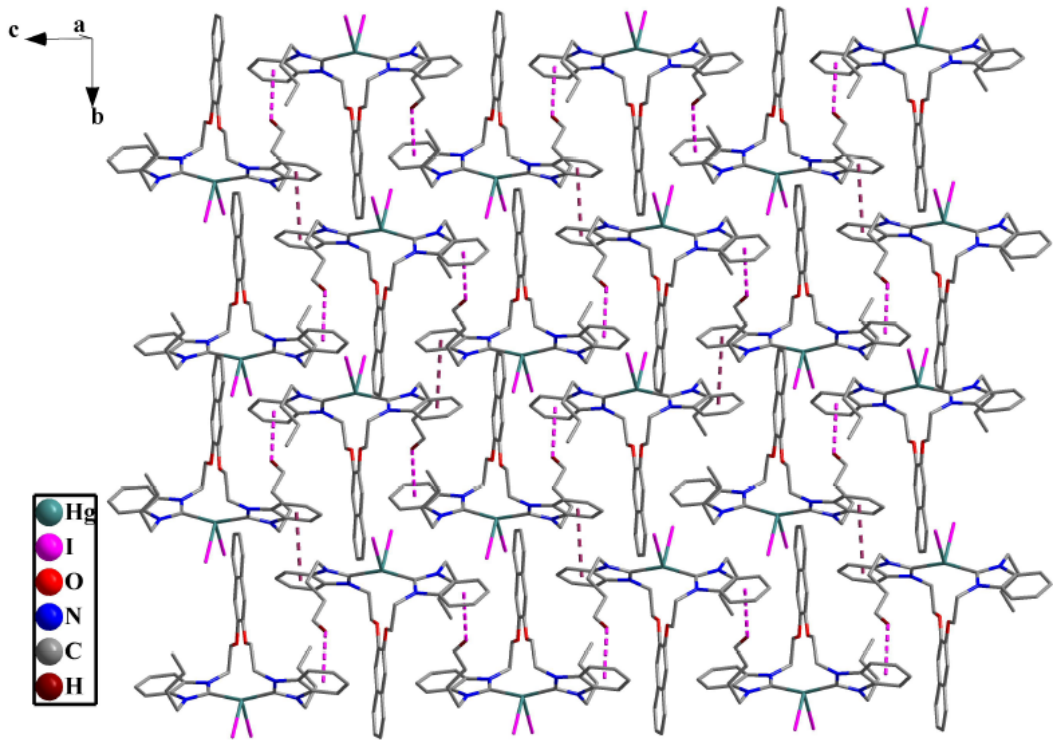

Fig. S4 2D supramolecular layer of complex **4** via π-π stacking interactions and C-H···π contacts. All hydrogen atoms except those participating in C-H···π hydrogen bonds were omitted for clarity.

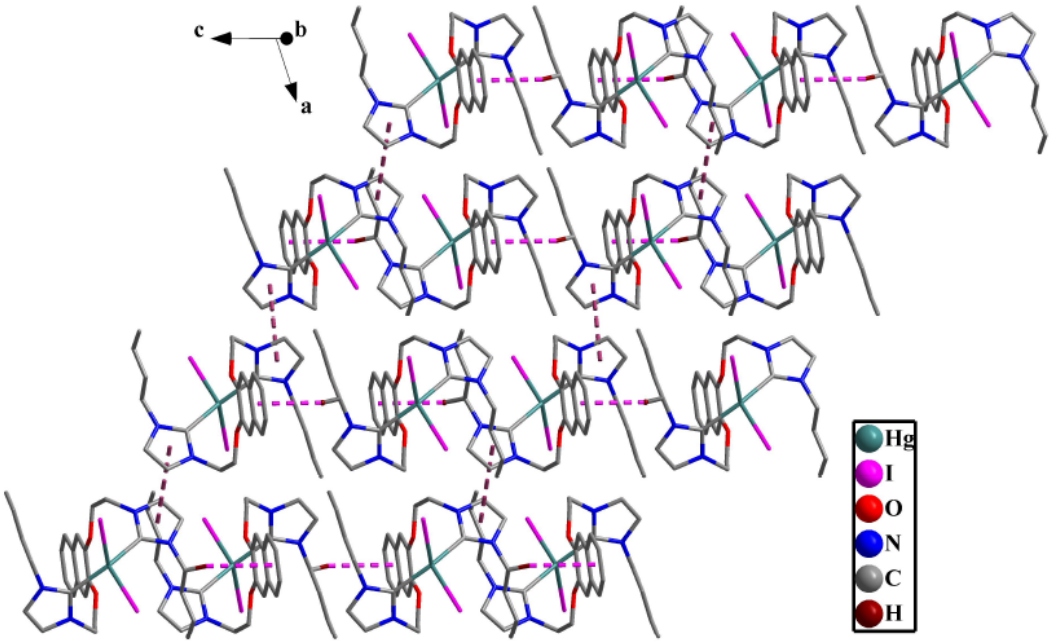

Fig. S5(a) 2D supramolecular layer of complex **5** via C-H···π contacts and π-π stacking interactions. All hydrogen atoms except those participating in C-H···π hydrogen bonds were omitted for clarity.

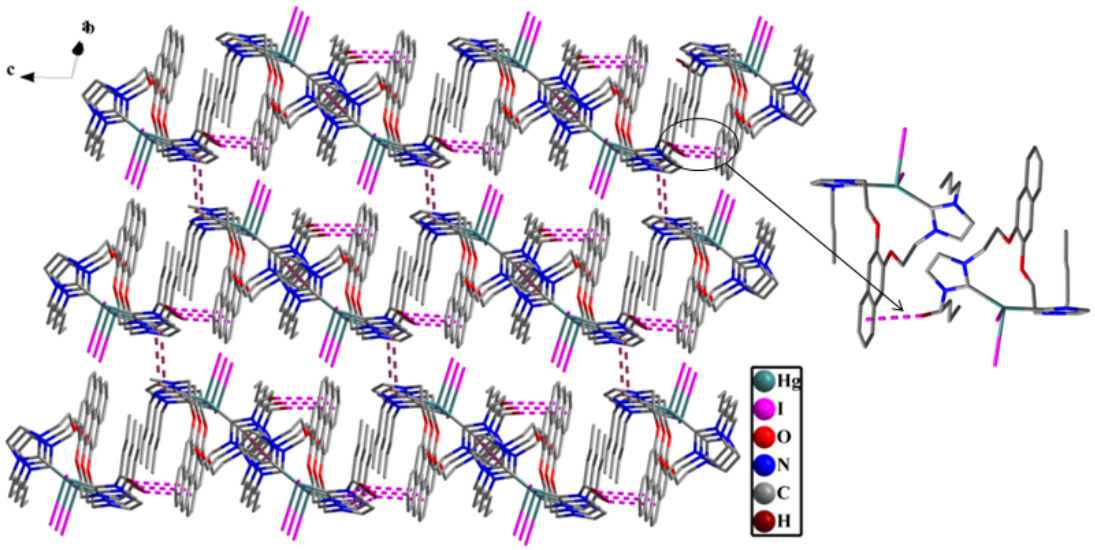

Fig. S5(b) 3D supramolecular network of complex **5** via π-π stacking interactions and C-H···π contacts. All hydrogen atoms except those participating in C-H···π hydrogen bonds were omitted for clarity.

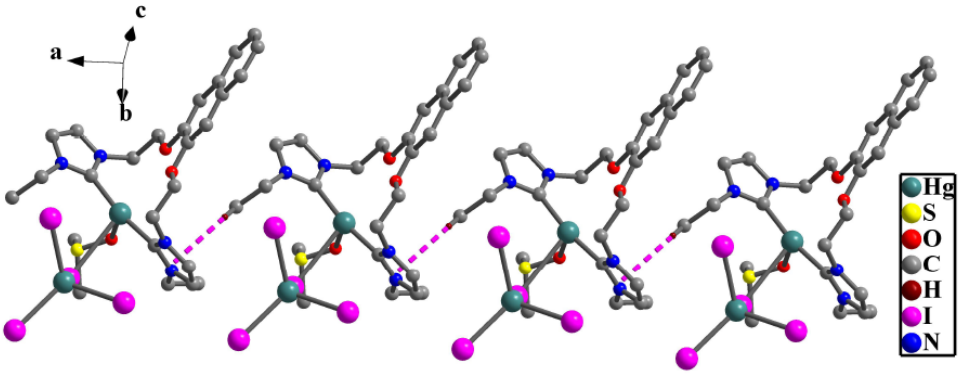

Fig. S6 1D chain of complex **6** via C-H···π contacts. All hydrogen atoms except those participating in C-H···π hydrogen bonds were omitted for clarity.

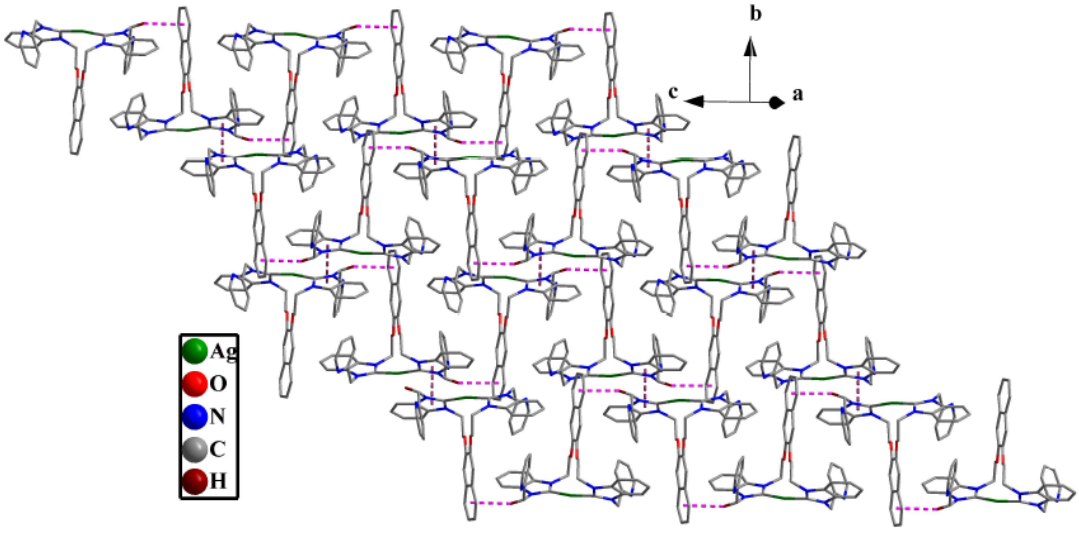

Fig. S7(a) 2D supramolecular layer of complex **7** via π-π stacking interactions and C-H···π contacts. All hydrogen atoms except those participating in C-H···π hydrogen bonds were omitted for clarity.

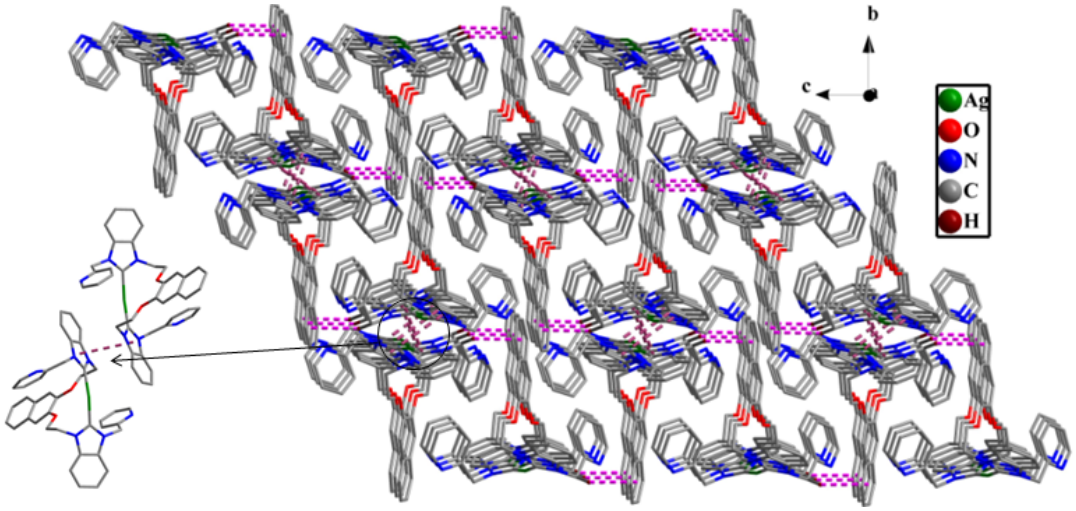

Fig. S7(b) 3D supramolecular network of complex **7** π-π stacking interactions and C-H···π contacts. All hydrogen atoms except those participating in C-H···π hydrogen bonds were omitted for clarity.

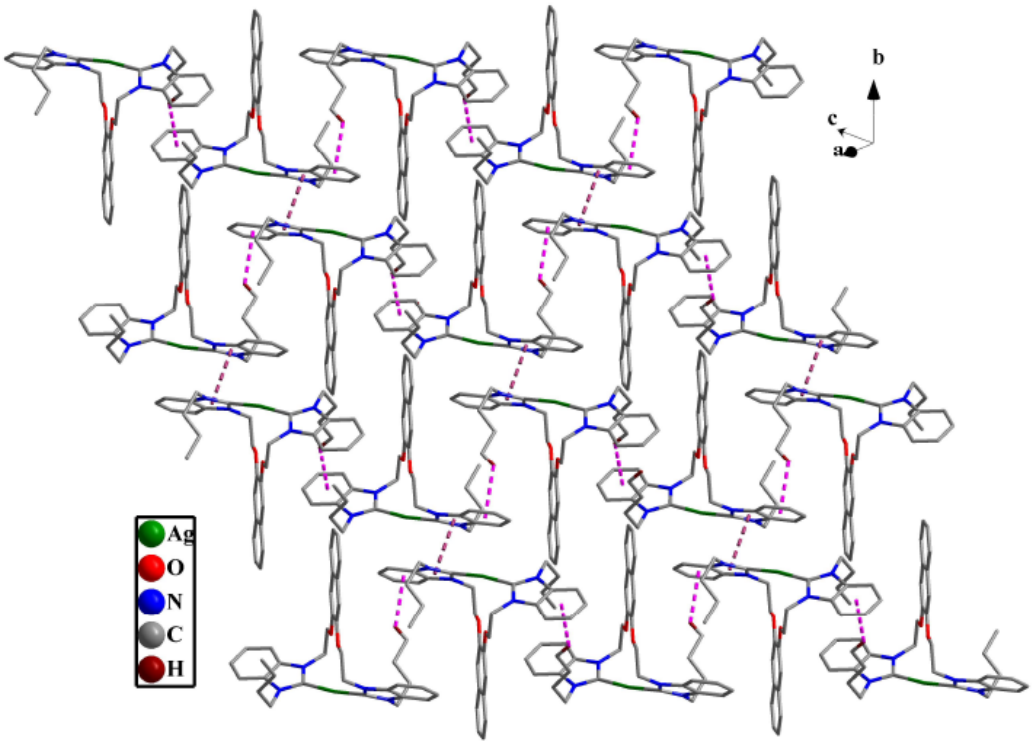

Fig. S8(a) 2D supramolecular layer of complex **8** via C-H···π contacts and π-π stacking interactions. All hydrogen atoms except those participating in C-H···π hydrogen bonds were omitted for clarity.

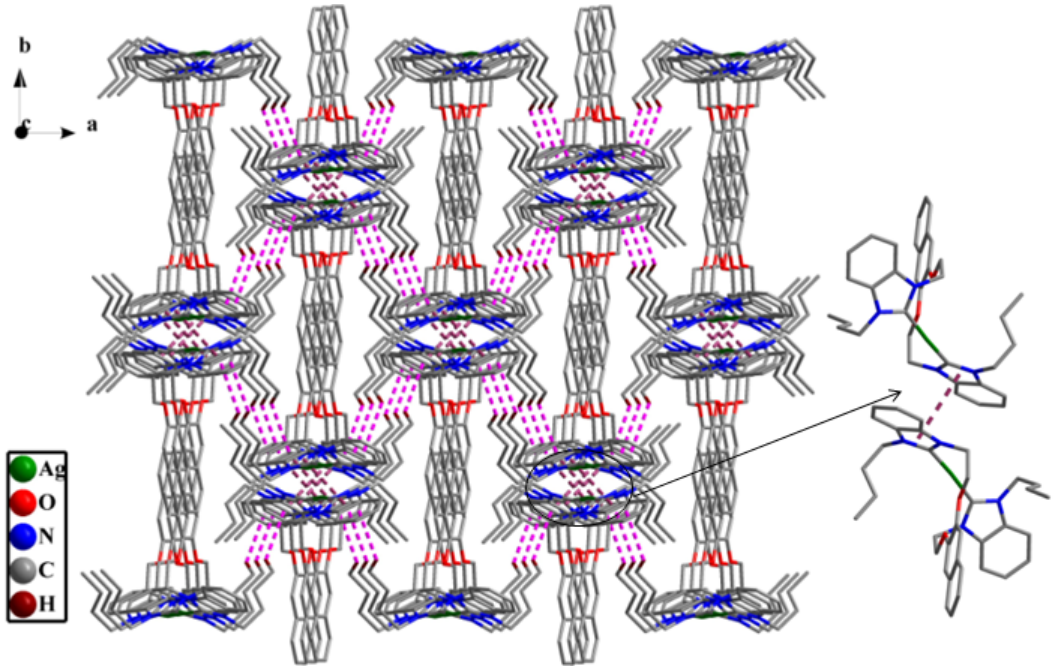

Fig. S8(b) 3D supramolecular network of complex **8** via C-H···π contacts and π-π stacking interactions. All hydrogen atoms except those participating in C-H···π hydrogen bonds were omitted for clarity.

6. The UV/Vis and fluorescence studies of complex 4

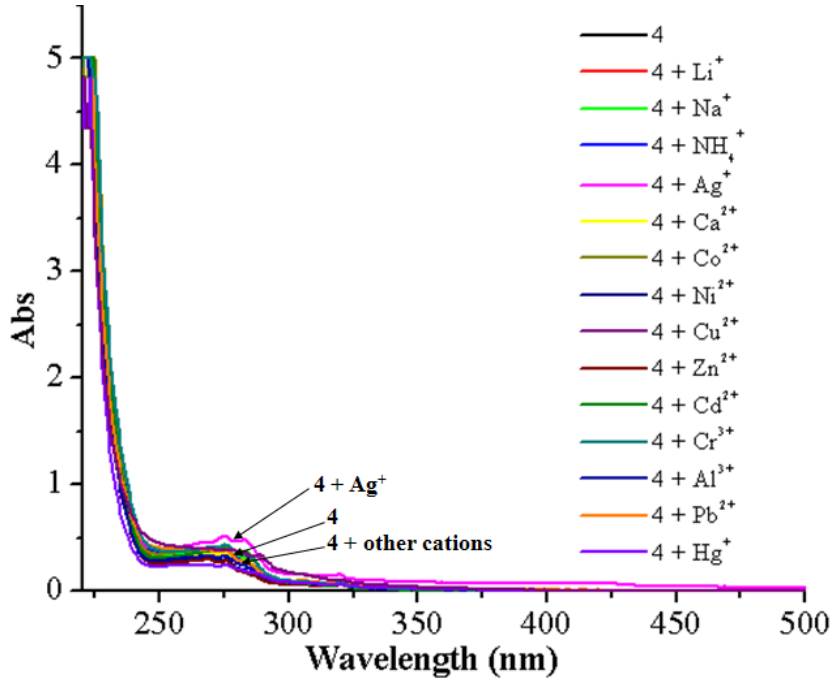

Fig. S9 UV-vis absorption spectra of **4** (1×10^{-5} mol/L) and upon the addition of salts (30.0 equiv) of Li^+, Na^+, NH_4^+, Ag^+, Ca^{2+}, Co^{2+}, Ni^{2+}, Cu^{2+}, Zn^{2+}, Cd^{2+}, Cr^{3+}, Al^{3+}, Pb^{2+} and Hg^{2+} in CH_3OH at 25 ˚C.

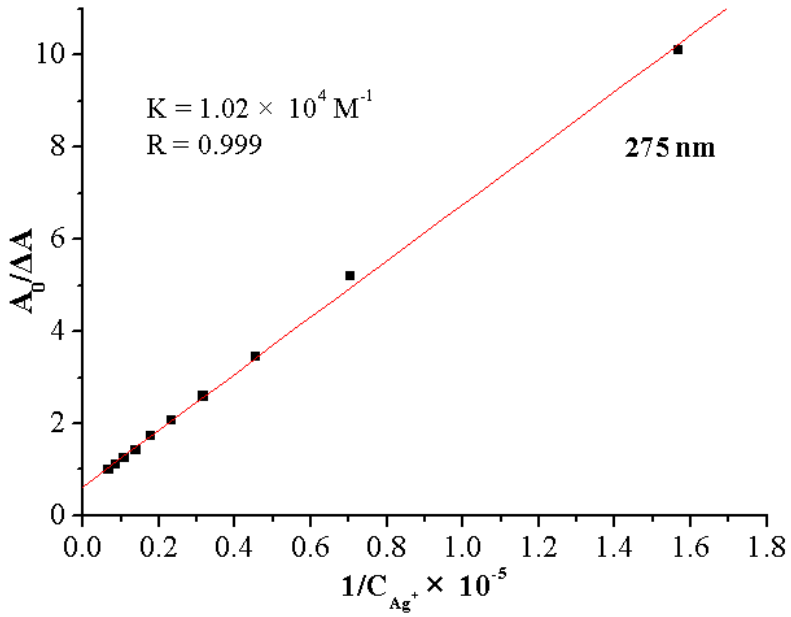

Fig. S10 Benesi-Hildebrand analysis of the absorption changes for the complexation between **4** and Ag^+ in CH_3OH at 25 ˚C.

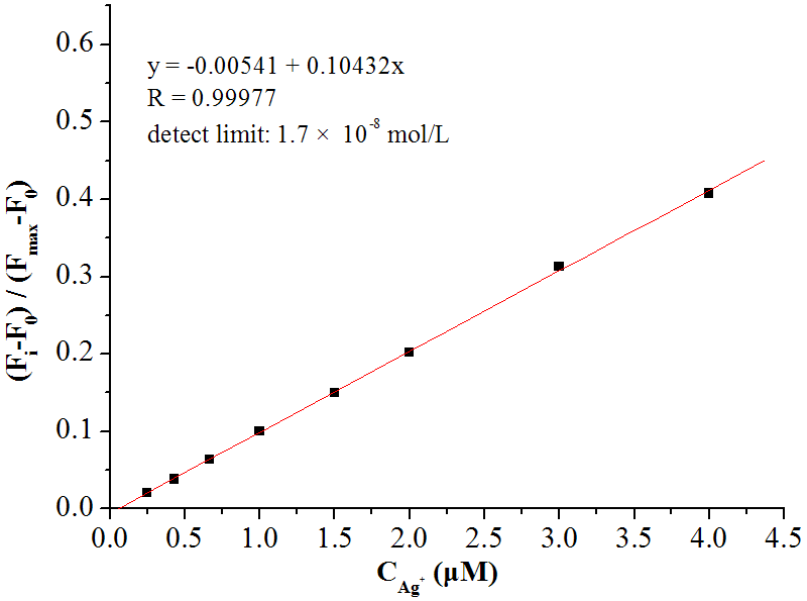

Fig. S11 Emission (at 338 nm) of **4** at different concentrations of Ag^+ (0, 0.25, 0.43, 0.67, 1.0, 1.5, 2.0, 3.0, 4.0 μM) added, normalized between the minimum emission (0.0 μM Ag^+) and the emission at 4.0 μM Ag^+ in CH_3OH at 25 ˚C. The detection limit was determined to be 1.7×10^{-8} M.

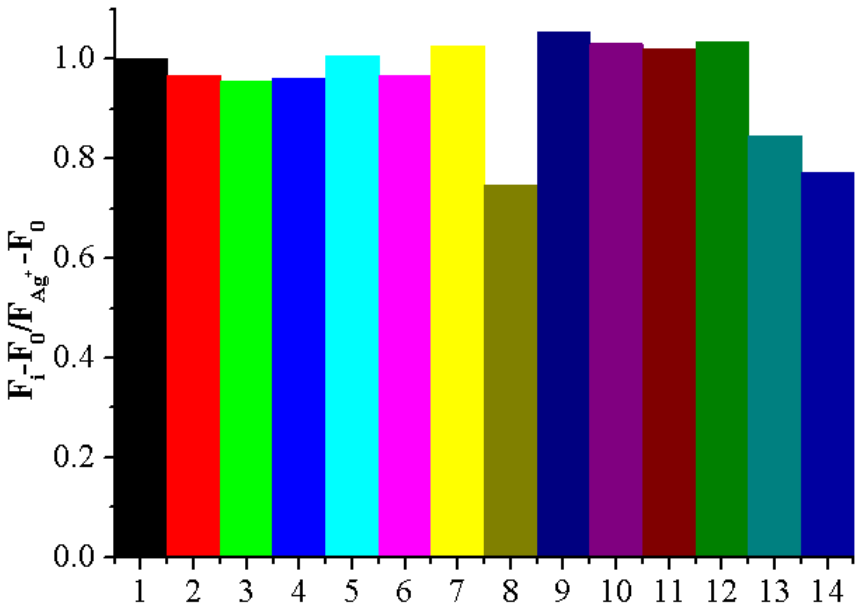

Fig. S12 Change ratio $((F_i-F_0)/(F_{Ag^+}-F_0)$ of fluorescence intensity of **4** upon addition of 30 equiv of Ag^+ in the presence of 30 equiv of background anions. 1: Ag^+; 2: Ag^+ + Li^+; 3: Ag^+ + Na^+; 4: Ag^+ + NH_4^+; 5: Ag^+ + Ca^{2+}; 6: Ag^+ + Co^{2+}; 7: Ag^+ + Ni^{2+}; 8: Ag^+ + Cu^{2+}; 9: Ag^+ + Zn^{2+}; 10: Ag^+ + Cd^{2+}; 11: Ag^+ + Cr^{3+}; 12: Ag^+ + Al^{3+}; 13: Ag^+ + Pb^{2+}; 14: Ag^+ + Hg^{2+} in CH_3OH at 25 ˚C.

7. The infrared spectra of complex 4 and 4·$AgNO_3$

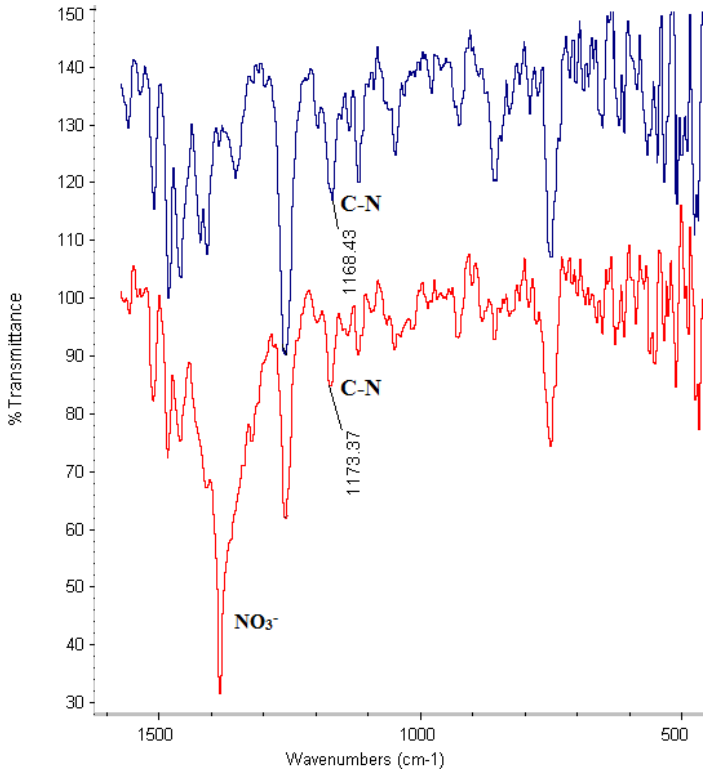

Fig. S13 Infrared spectroscopy of complex **4** (top) and **4**·Ag^+ (bottom).

8. The ^{1}H NMR and ^{13}C NMR spectra of precursors and complexes 1-8

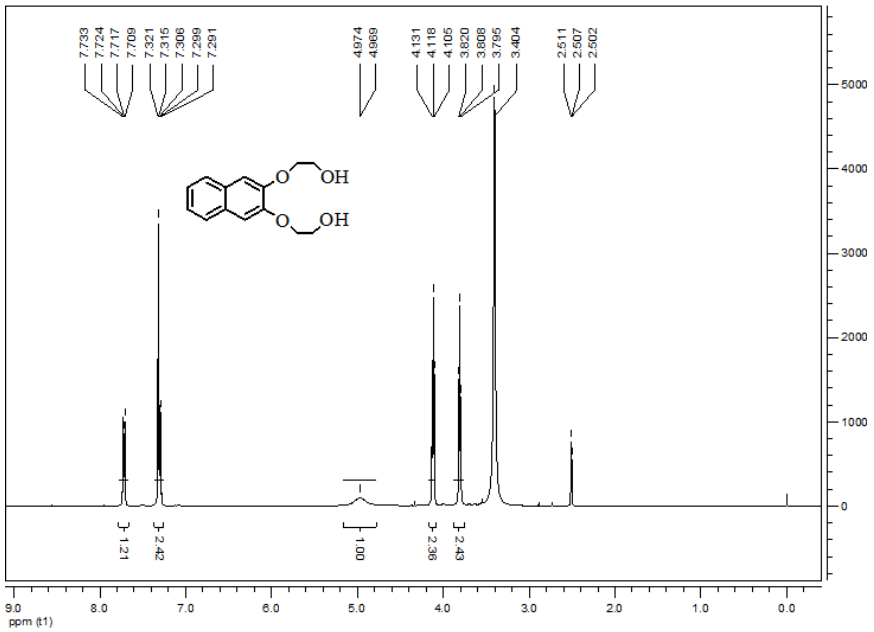

Fig. S14 The ^{1}H NMR (400 MHz, DMSO-d_6) spectra of 2,3-bis(2'-hydroxyethoxy)naphthalene.

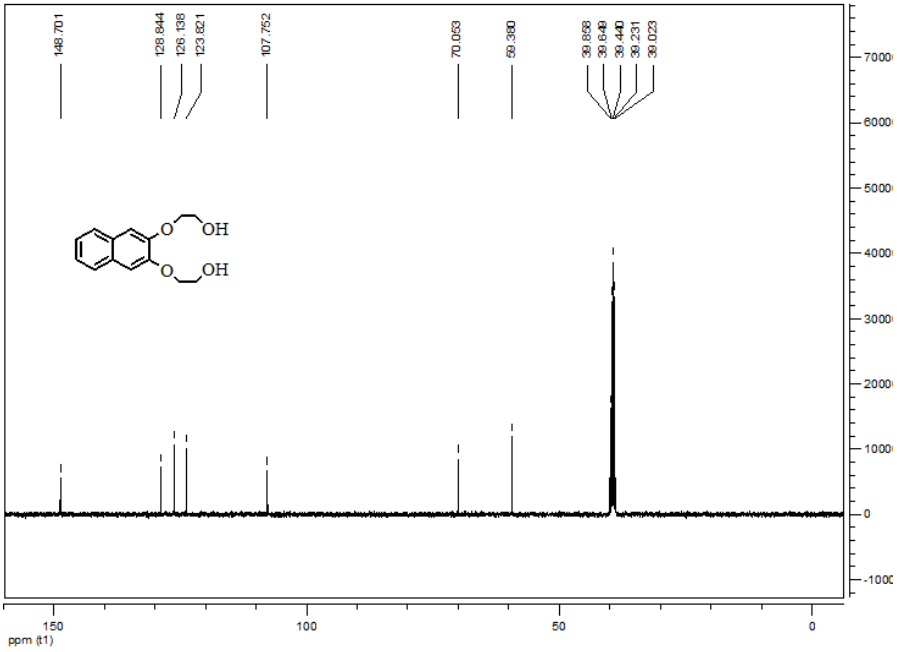

Fig. S15 The ^{13}C NMR (400 MHz, DMSO-d_6) spectra of 2,3-bis(2'-hydroxyethoxy)naphthalene.

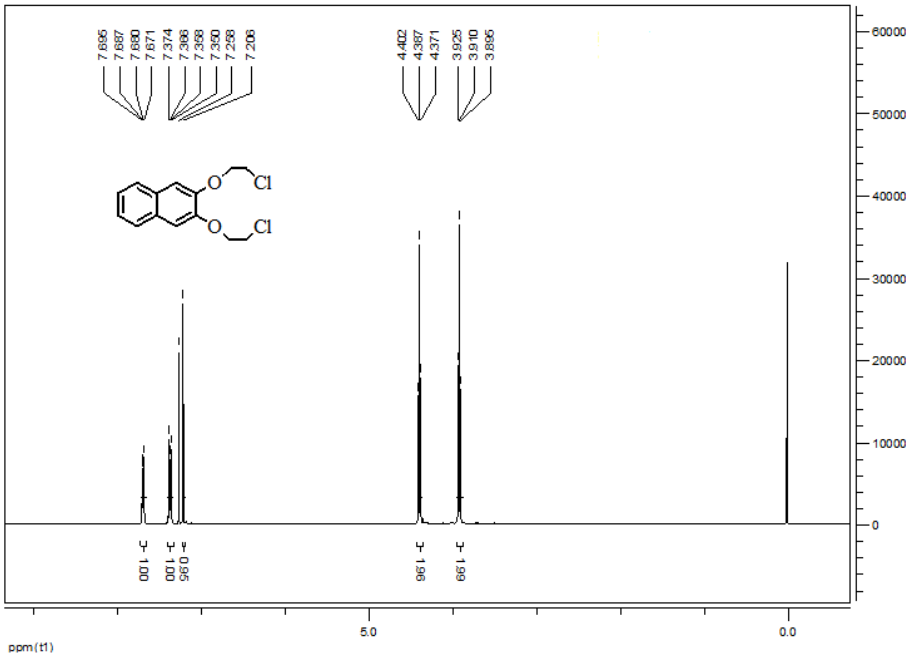

Fig. S16 The ^{1}H NMR (400 MHz, $CDCl_3$) spectra of 2,3-bis(2'-chloroethoxy)naphthalene.

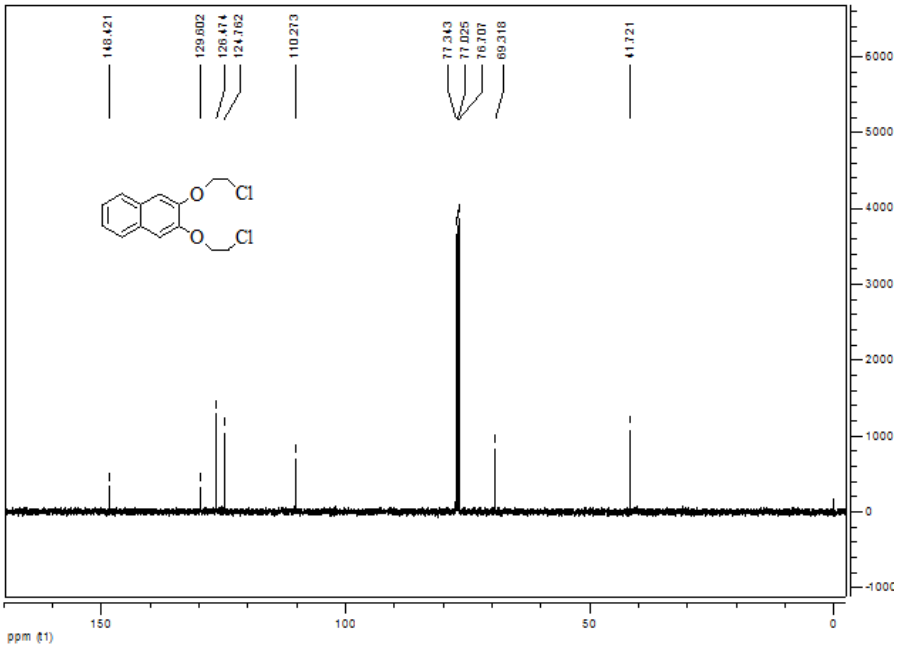

Fig. S17 The ^{13}C NMR (100 MHz, $CDCl_3$) spectra of 2,3-bis(2'-chloroethoxy)naphthalene.

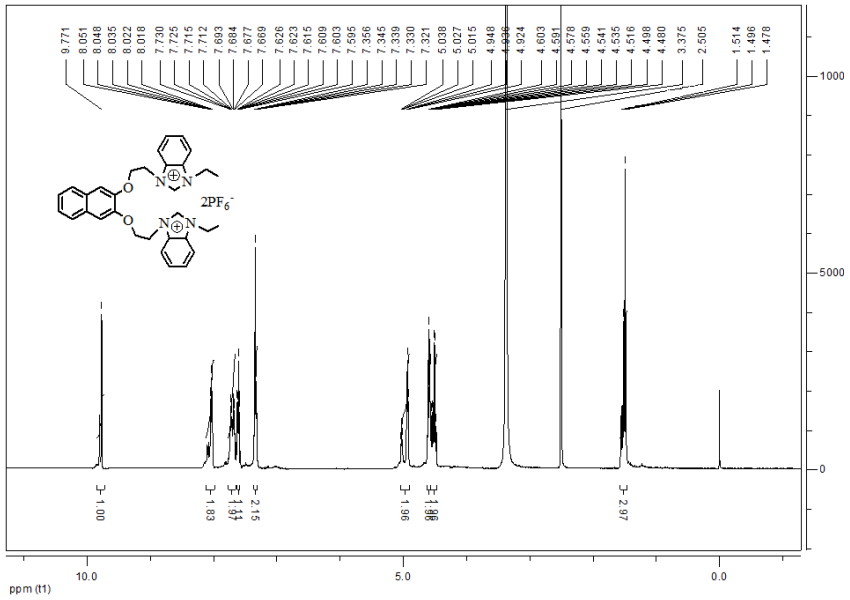

Fig. S18 The ^{1}H NMR (400 MHz, DMSO-d_6) spectra of $\mathbf{L^1H_2{\cdot}(PF_6)_2}$.

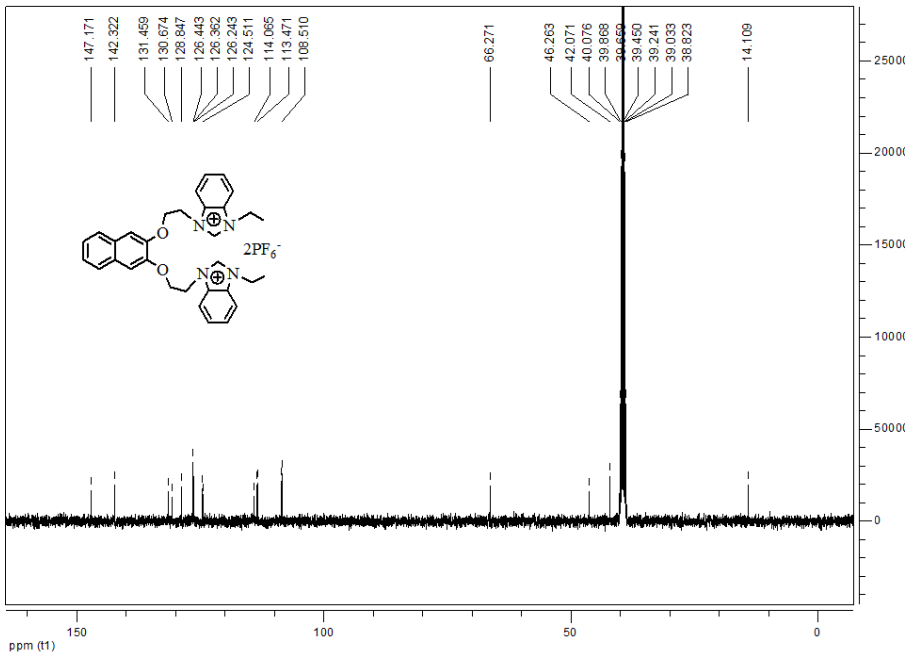

Fig. S19 The ^{13}C NMR (100 MHz, DMSO-d_6) spectra of $\mathbf{L^1H_2{\cdot}(PF_6)_2}$.

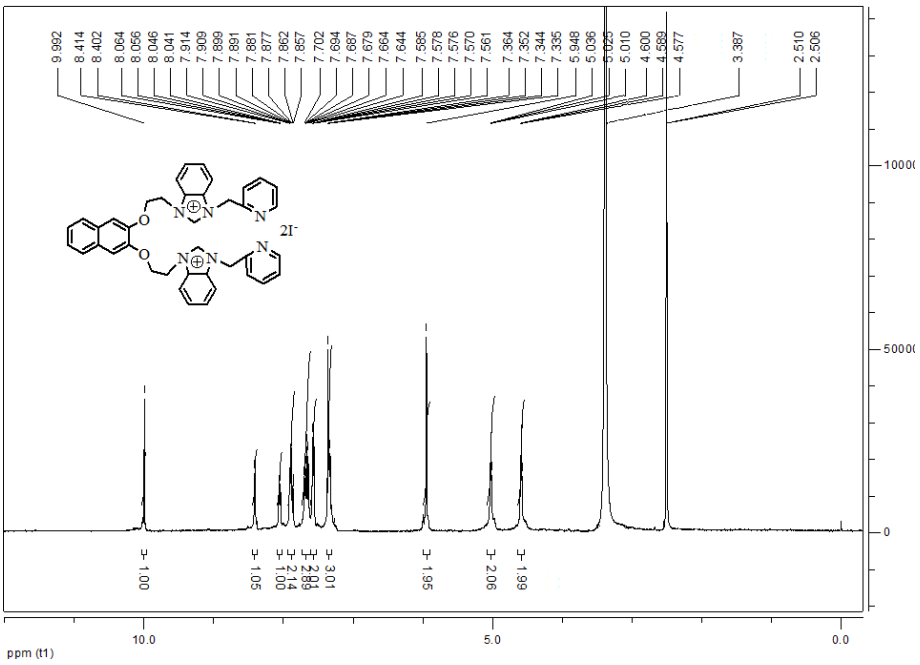

Fig. S20 The ^{1}H NMR (400 MHz, DMSO-d_6) spectra of $\mathbf{L^2H_2 \cdot I_2}$.

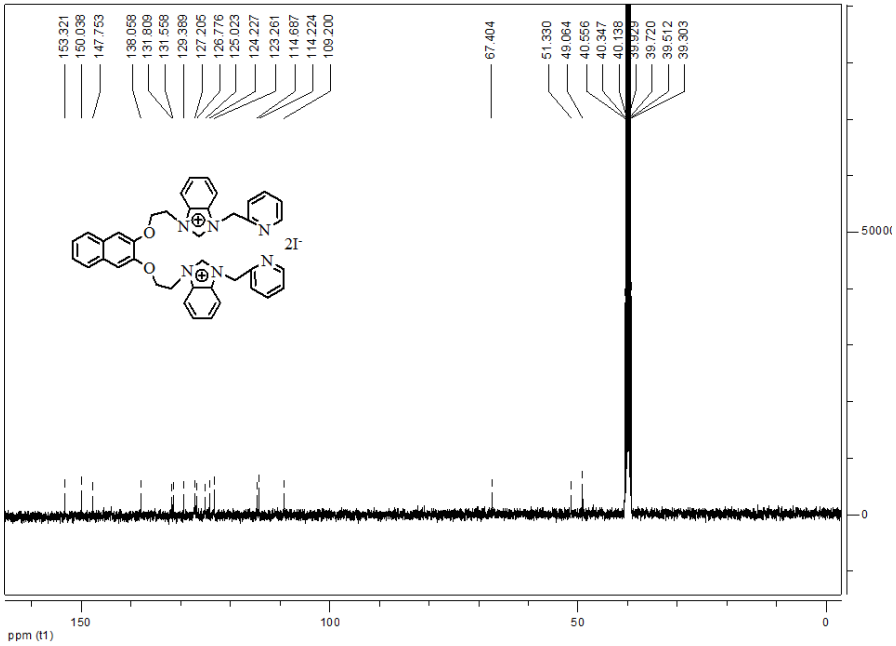

Fig. S21 The ^{13}C NMR (100 MHz, DMSO-d_6) spectra of $\mathbf{L^2H_2 \cdot I_2}$.

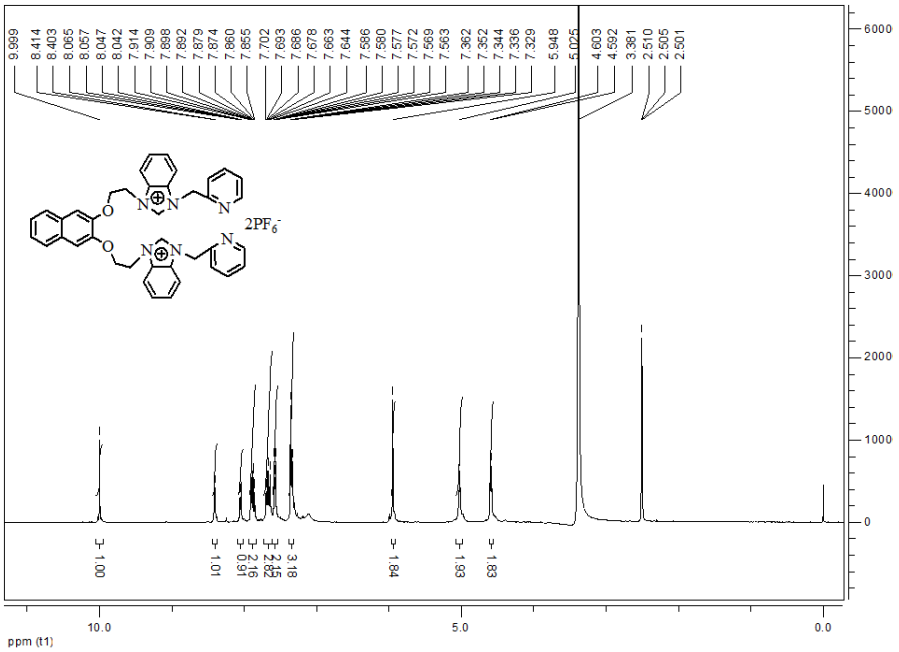

Fig. S22 The ^{1}H NMR (400 MHz, DMSO-d$_6$) spectra of $\mathbf{L^2H_2{\cdot}(PF_6)_2}$.

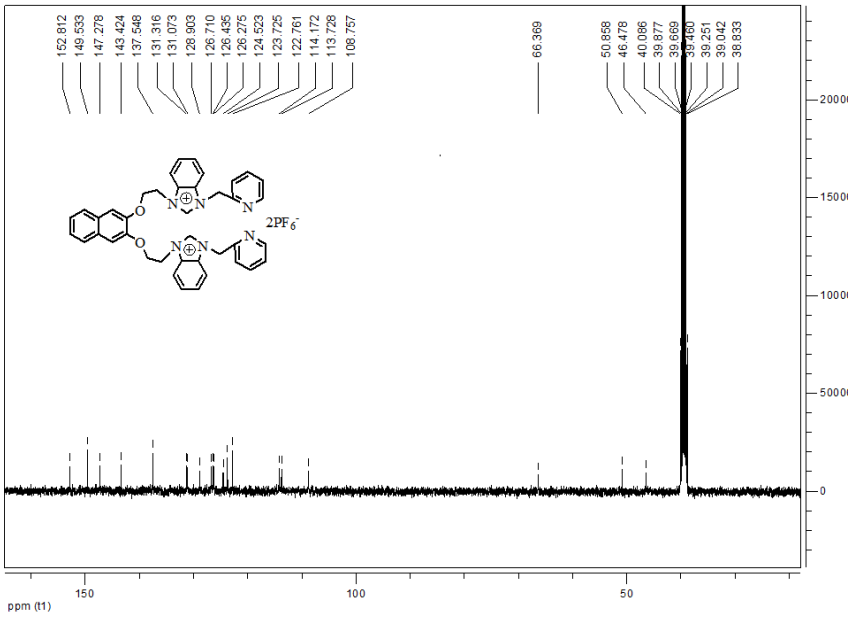

Fig. S23 The ^{13}C NMR (100 MHz, DMSO-d$_6$) spectra of $\mathbf{L^2H_2{\cdot}(PF_6)_2}$.

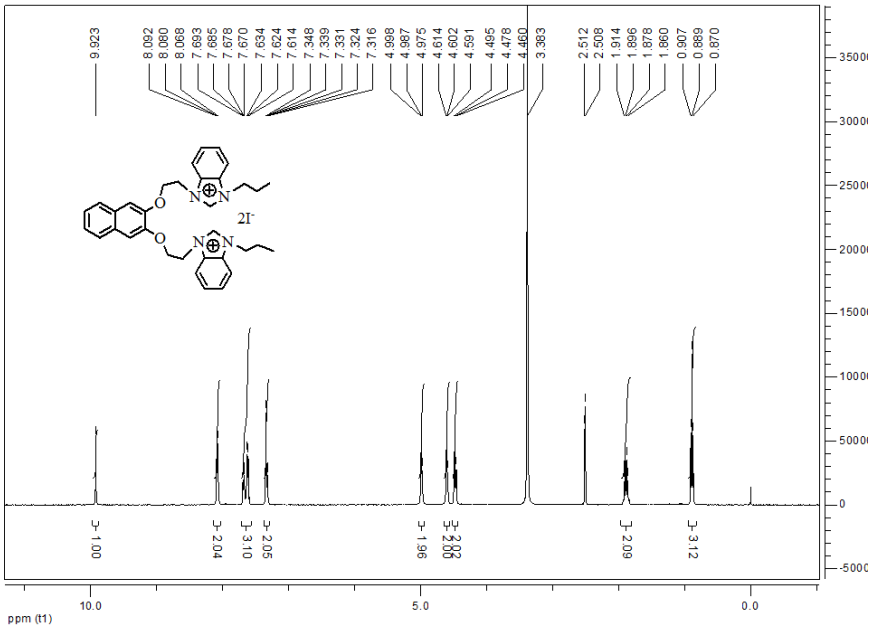

Fig. S24 The ^{1}H NMR (400 MHz, DMSO-d_6) spectra of $\mathbf{L^3H_2 \cdot I_2}$.

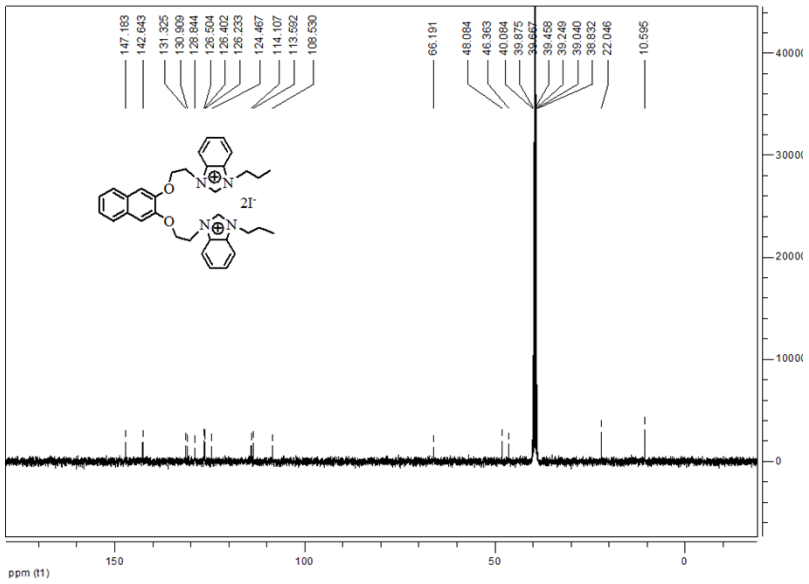

Fig. S25 The ^{13}C NMR (100 MHz, DMSO-d_6) spectra of $\mathbf{L^3H_2 \cdot I_2}$.

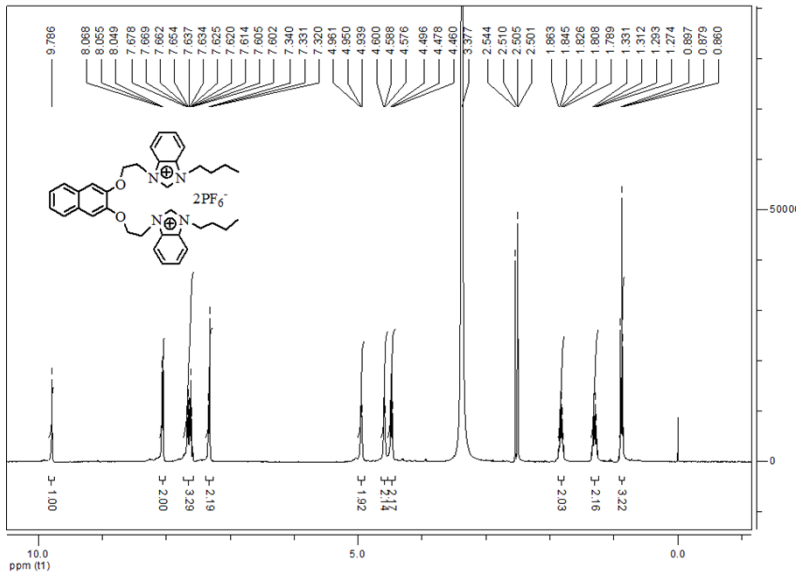

Fig. S26 The ^{1}H NMR (400 MHz, DMSO-d_6) spectra of $\mathbf{L^4H_2 \cdot (PF_6)_2}$.

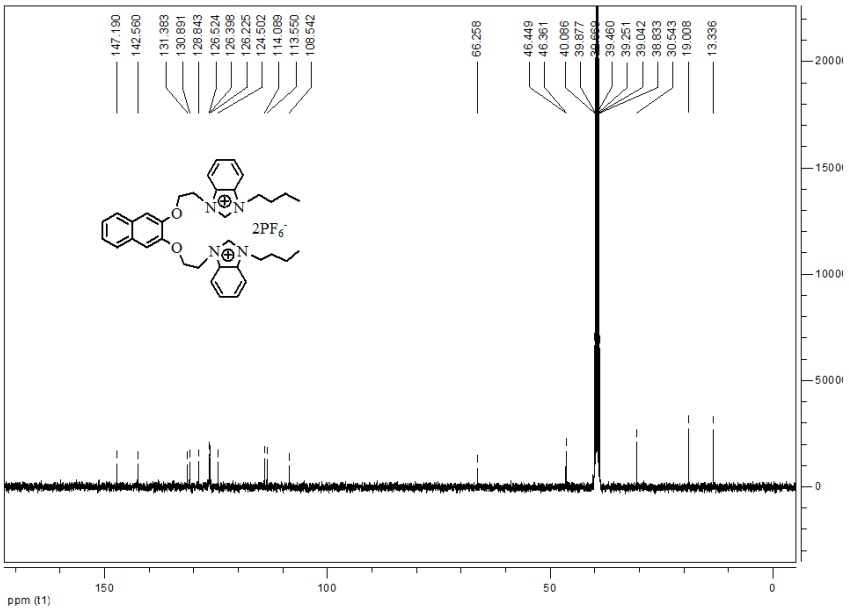

Fig. S27 The ^{13}C NMR (100 MHz, DMSO-d_6) spectra of $\mathbf{L^4H_2 \cdot (PF_6)_2}$.

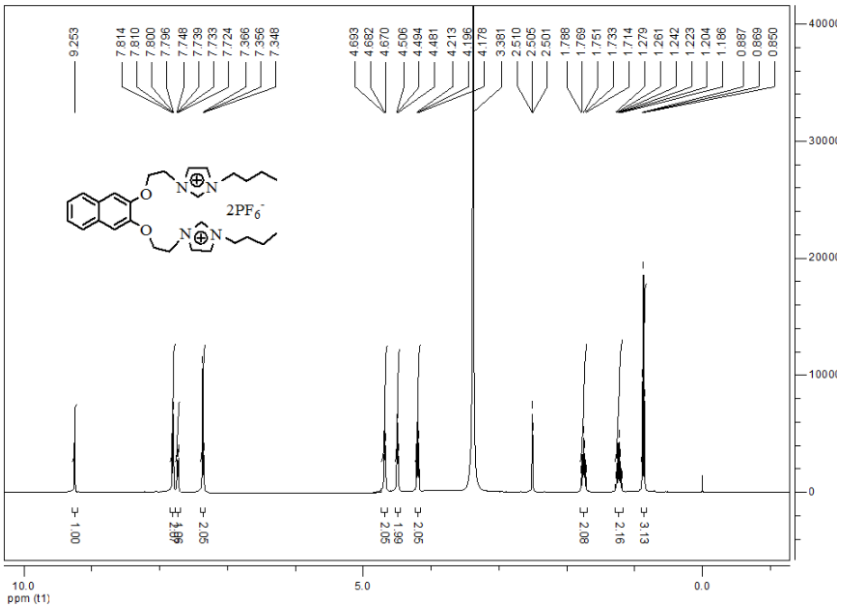

Fig. S28 The ^{1}H NMR (400 MHz, DMSO-d_6) spectra of $\mathbf{L^5H_2{\cdot}(PF_6)_2}$.

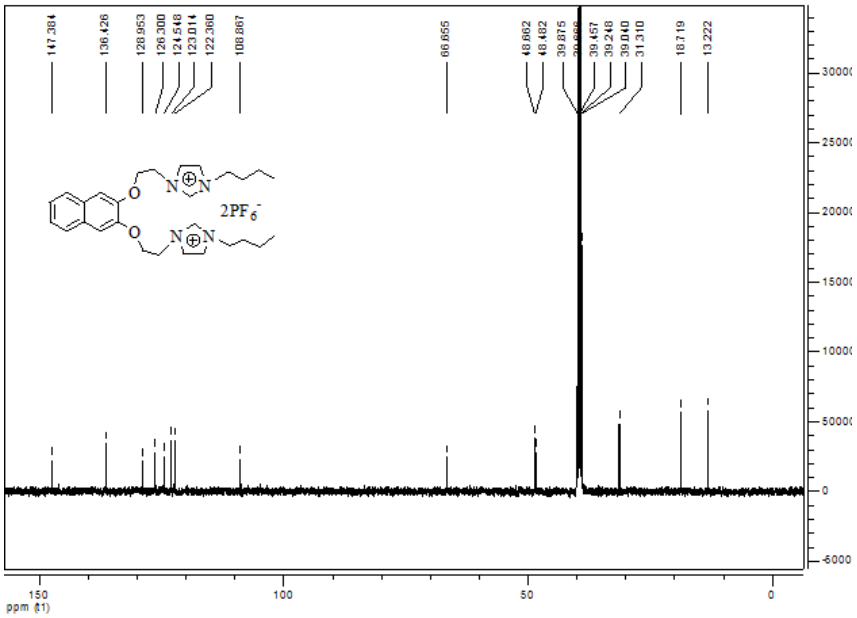

Fig. S29 The ^{13}C NMR (100 MHz, DMSO-d_6) spectra of $\mathbf{L^5H_2{\cdot}(PF_6)_2}$.

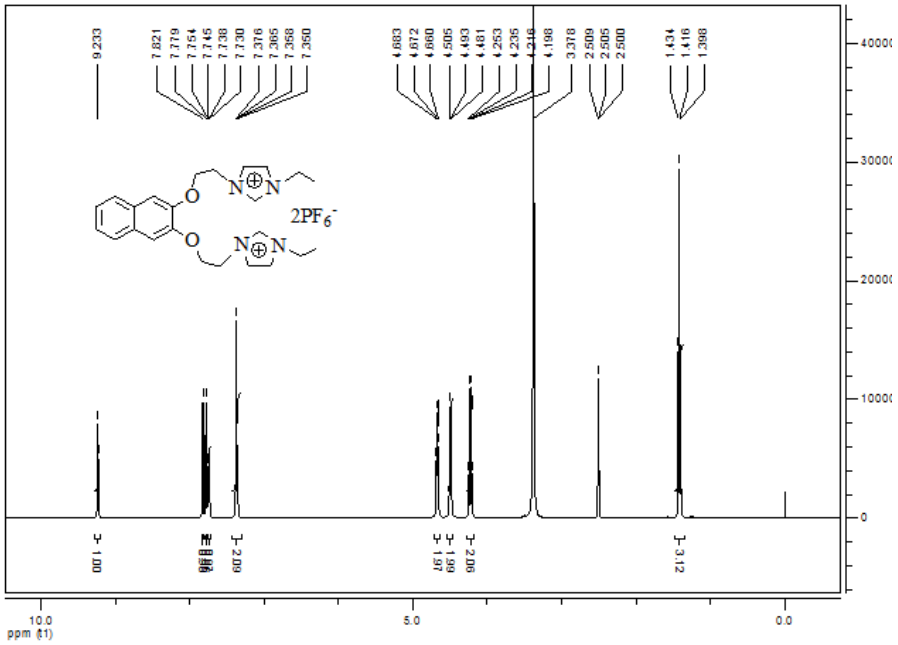

Fig. S30 The ^{1}H NMR (400 MHz, DMSO-d_6) spectra of $\mathbf{L^6H_2 \cdot (PF_6)_2}$.

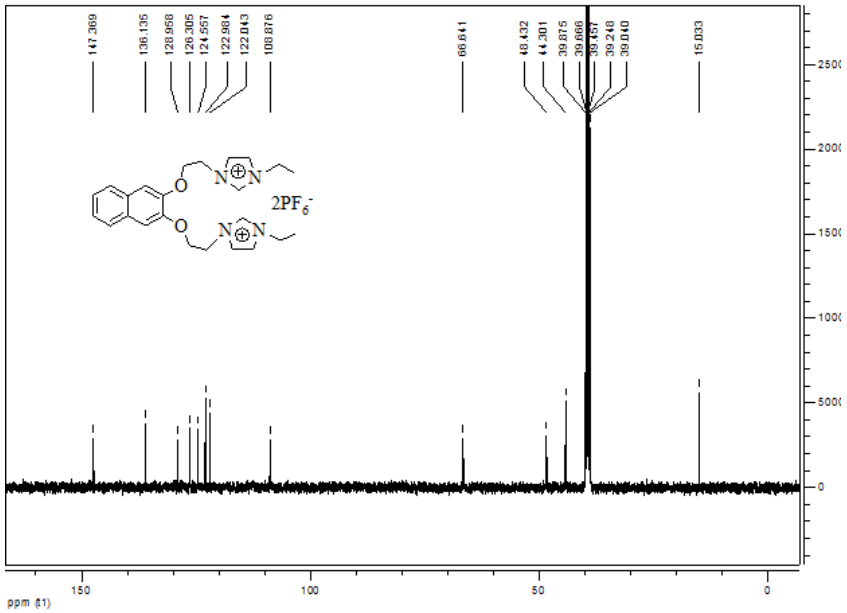

Fig. S31 The ^{13}C NMR (100 MHz, DMSO-d_6) spectra of $\mathbf{L^6H_2 \cdot (PF_6)_2}$.

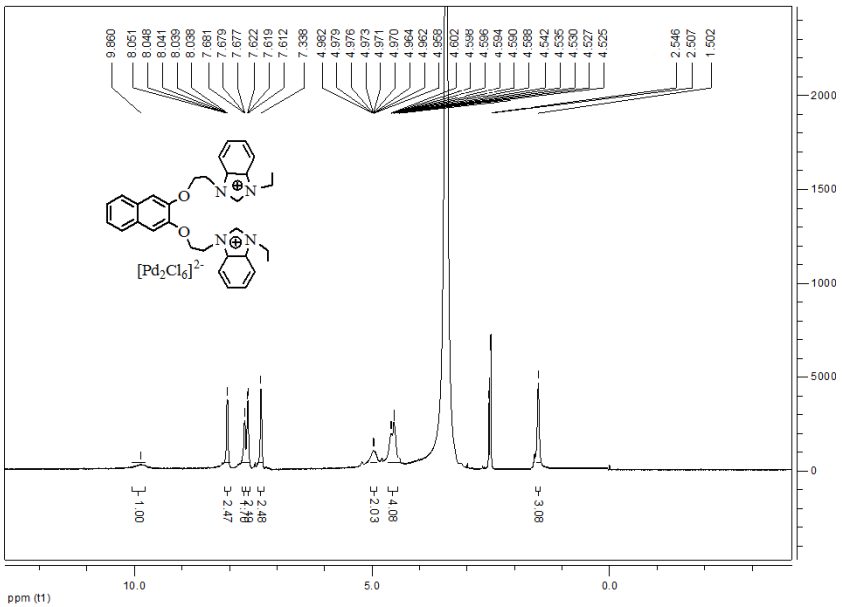

Fig. S32 The ^{1}H NMR (400 MHz, DMSO-d_6) spectra of **1**.

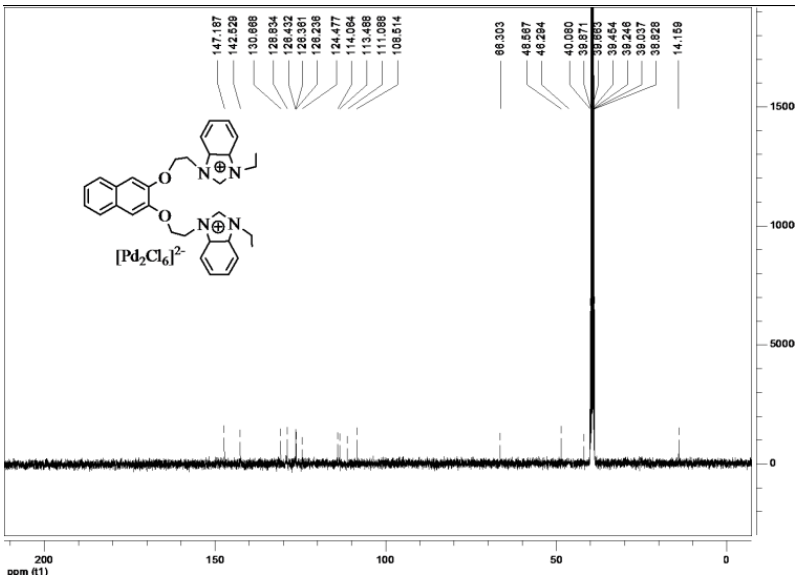

Fig. S33 The ^{13}C NMR (100 MHz, DMSO-d_6) spectra of **1**.

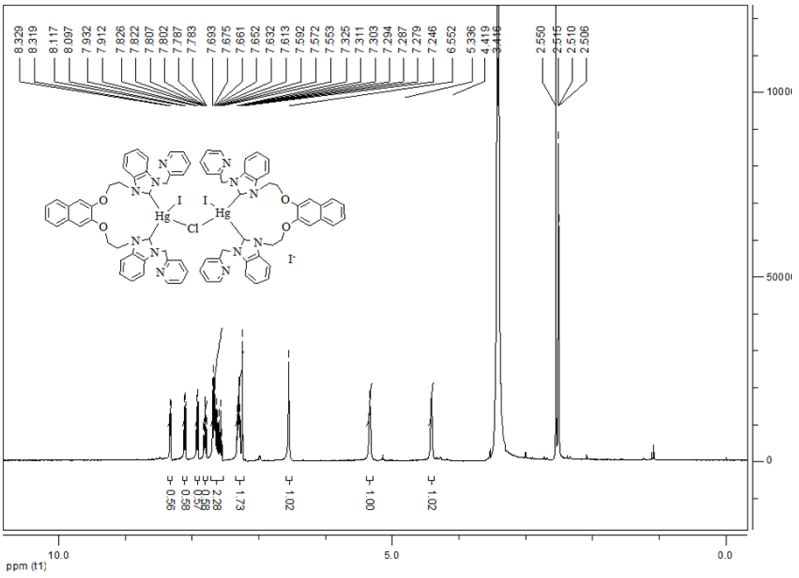

Fig. S34 The ^{1}H NMR (400 MHz, DMSO-d_6) spectra of **2**.

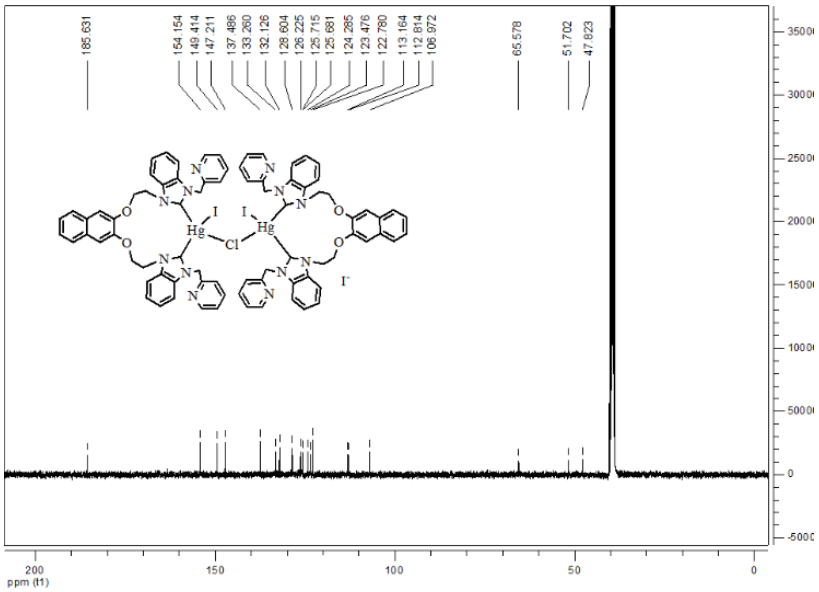

Fig. S35 The ^{13}C NMR (100 MHz, DMSO-d_6) spectra of **2**.

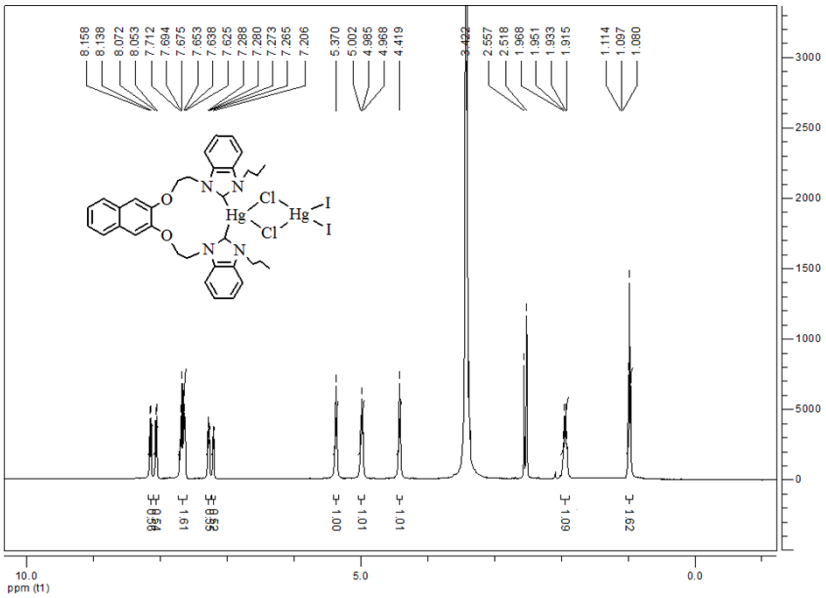

Fig. S36 The ^{1}H NMR (400 MHz, DMSO-d_6) spectra of **3**.

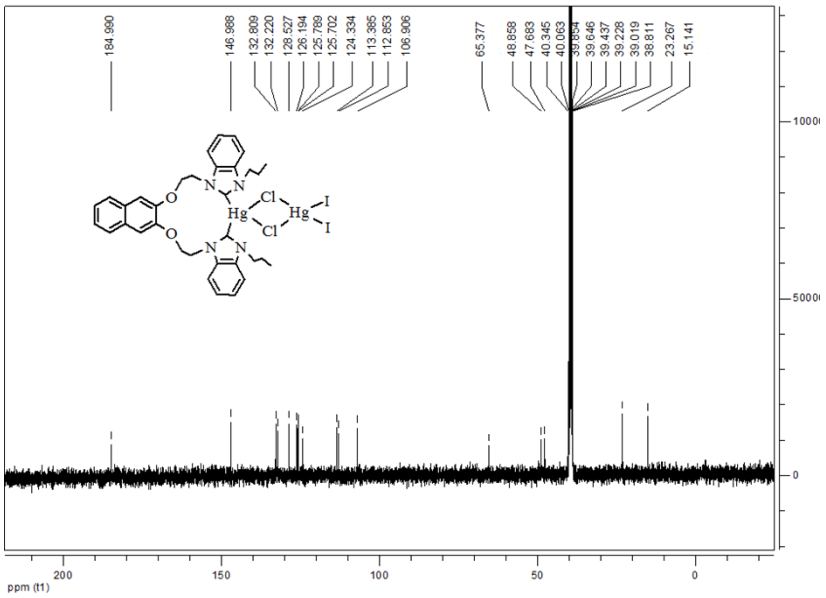

Fig. S37 The ^{13}C NMR (100 MHz, DMSO-d_6) spectra of **3**.

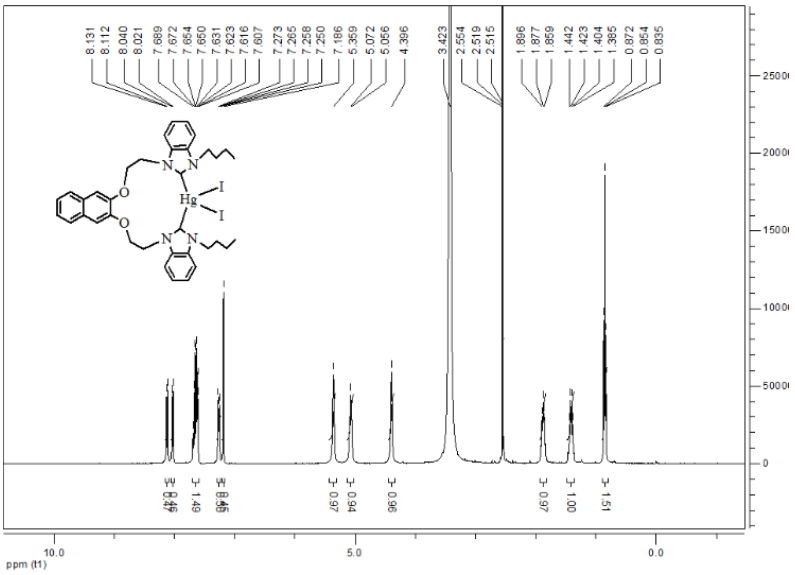

Fig. S38 The ^{1}H NMR (400 MHz, DMSO-d_6) spectra of **4**.

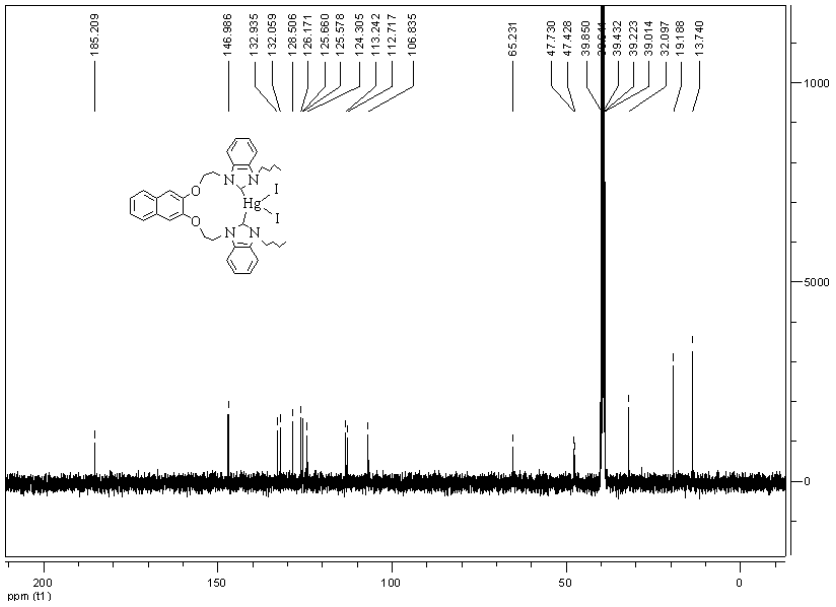

Fig. S39 The ^{13}C NMR (100 MHz, DMSO-d_6) spectra of **4**.

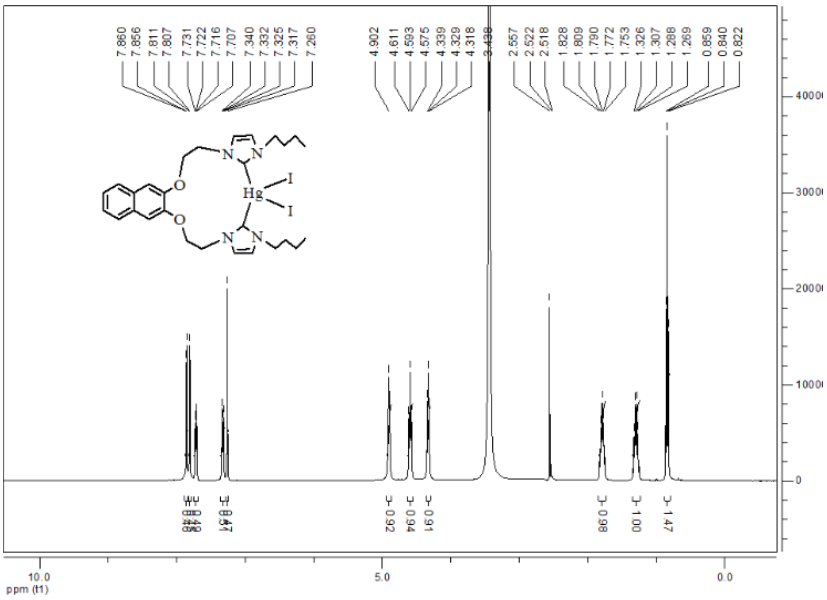

Fig. S40 The ^{1}H NMR (400 MHz, DMSO-d_6) spectra of **5**.

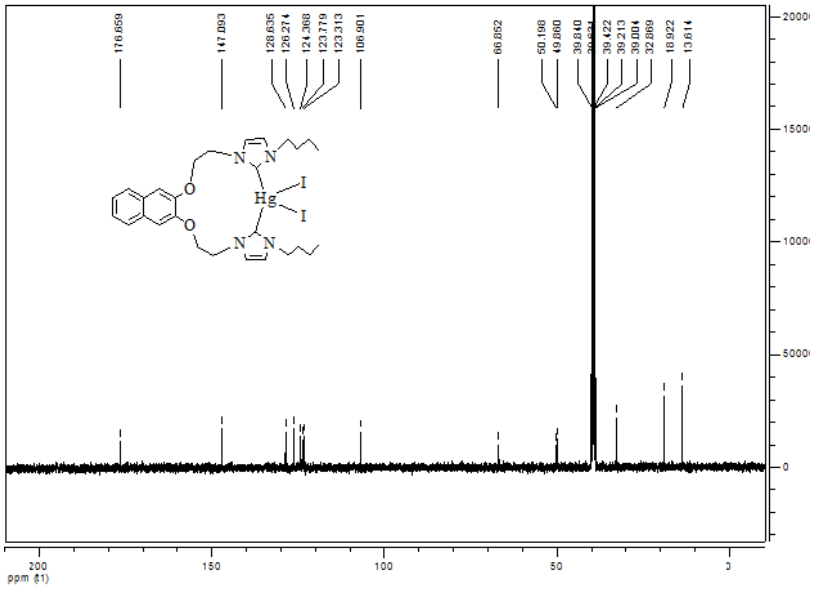

Fig. S41 The ^{13}C NMR (100 MHz, DMSO-d_6) spectra of **5**.

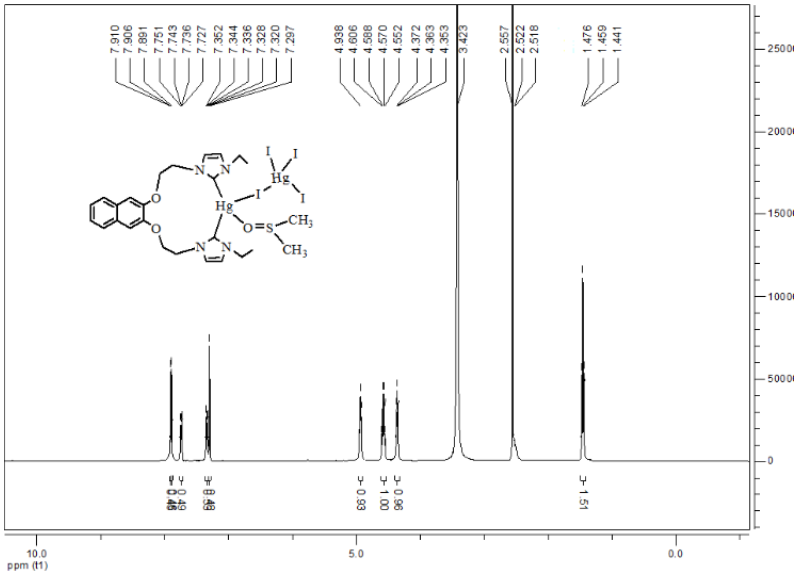

Fig. S42 The ^{1}H NMR (400 MHz, DMSO-d_6) spectra of **6**.

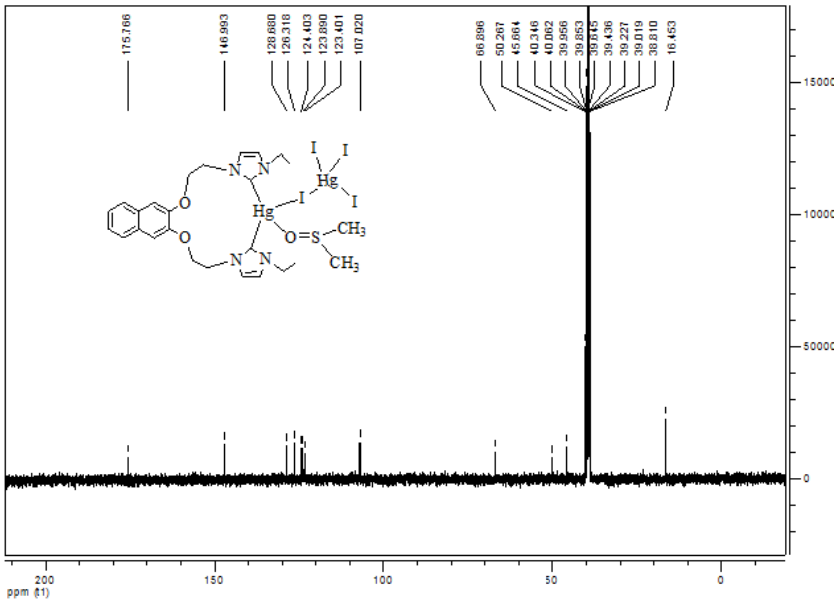

Fig. S43 The ^{13}C NMR (100 MHz, DMSO-d_6) spectra of **6**.

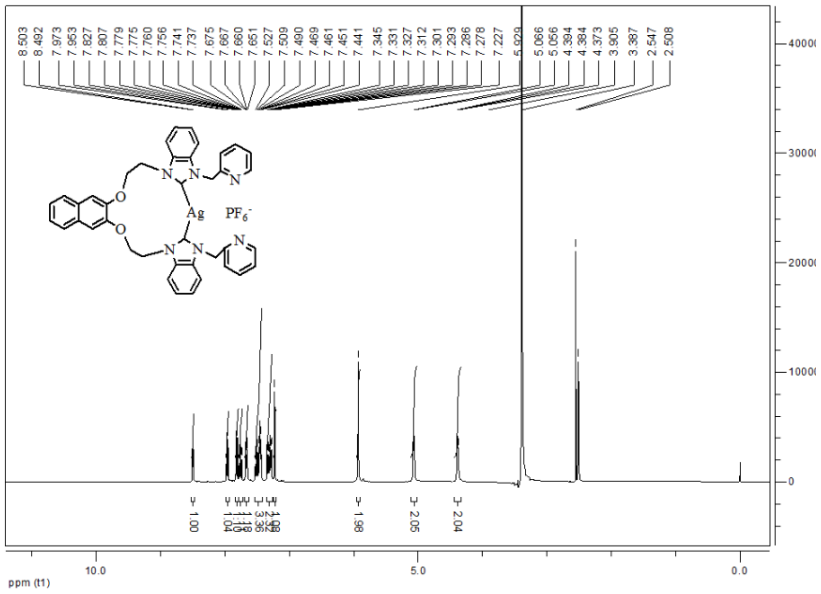

Fig. S44 The ^{1}H NMR (400 MHz, DMSO-d_6) spectra of **7**.

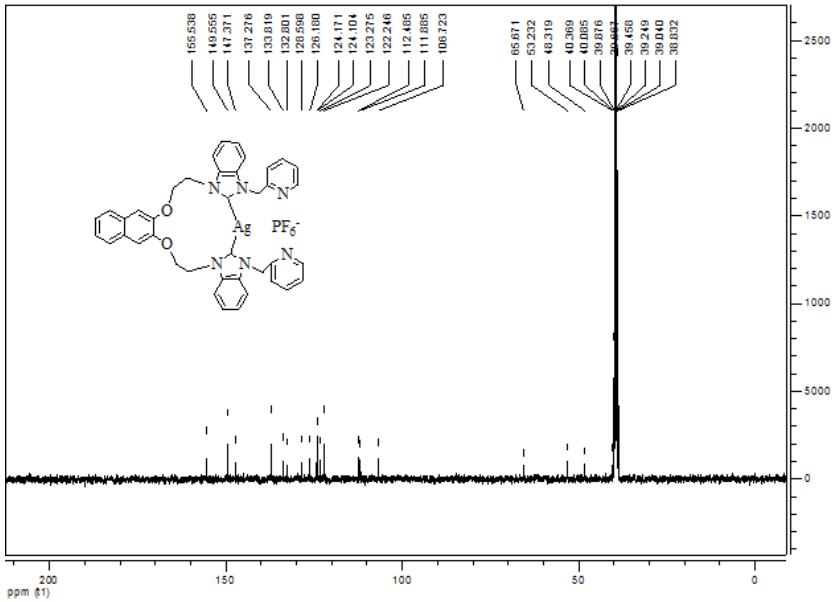

Fig. S45 The ^{13}C NMR (100 MHz, DMSO-d_6) spectra of **7**.

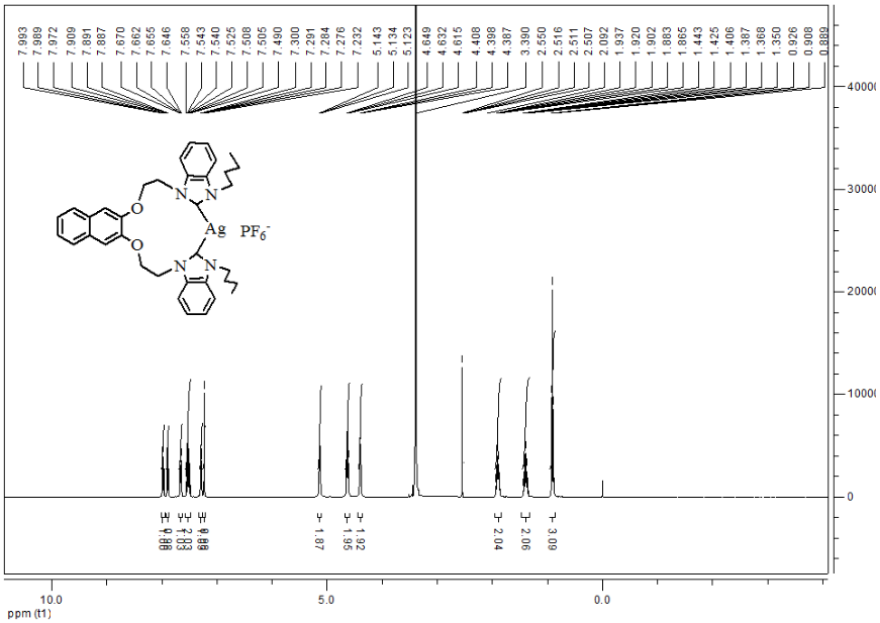

Fig. S46 The ^{1}H NMR (400 MHz, DMSO-d_6) spectra of **8**.

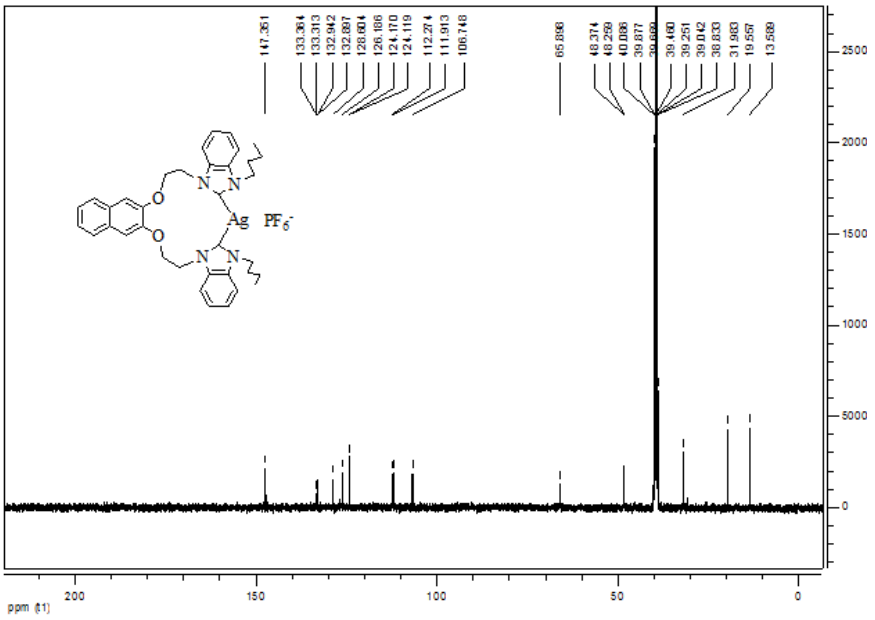

Fig. S47 The ^{13}C NMR (100 MHz, DMSO-d_6) spectra of **8**.